Ocean Engineering 286 (2023) 115584

Contents lists available at ScienceDirect

Ocean Engineering

journal homepage: www.elsevier.com/locate/oceaneng

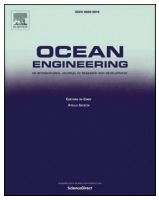

Effect of floater flexibility on global dynamic responses of a 15-MW semi-submersible floating wind turbine

Haoran Li [a,b], Zhen Gao [b,c,*], Erin E. Bachynski-Polić [b], Yuna Zhao [d], Stian Fiskvik [d]

[a] College of Harbor, Coastal and Offshore Engineering, Hohai University, Nanjing, 210024, China
[b] Department of Marine Technology, Norwegian University of Science and Technology, Trondheim, 7491, Norway
[c] School of Naval Architecture, Ocean and Civil Engineering, Shanghai Jiao Tong University, Shanghai, 200240, China
[d] COWI Energy International, COWI, Norway

ARTICLE INFO

Handling Editor: Prof. A.I. Incecik

Keywords:
Semi-submersible floating wind turbine
Floater flexibility
Dynamic response
Hydrodynamic model
Structural model

ABSTRACT

Floater structural flexibility plays a significant role in accurate predictions of global dynamic responses of floating wind turbines (FWTs), especially for ultra-large wind turbines with increasing size and cost-effective floater design. The conventional analysis of FWTs often considers the floater as one rigid body, which cannot capture the correct resonant responses of the floater (especially the column that supports the tower). In this paper, a new approach where the floater is divided into multiple rigid bodies connected by flexible beams is developed for advanced modelling of flexible floaters in combination with coupled time-domain simulations. The hydrostatic and hydrodynmaic loads on each body from a one-body hydrodynamic analysis, together with gravitational loads and inertial loads, are implemented in the beam-based finite element model of the floater to carry out a time-domain analysis. The proposed approach is used to compare the responses of a 15-MW semi-submersible FWT considering a rigid and a flexible floater. The inclusion of floater flexibility reduces the tower natural frequency. It leads to larger bending moment amplitudes at the tower base close to the tower bending natural frequency, particularly in only-wind, irregular wave and wind-wave conditions, but smaller dynamic responses in regular wave conditions.

1. Introduction

Floating wind turbines (FWTs) have been considered as the preferred solution for harnessing the wind energy in intermediate and deep seas where there is great potential for power production (Musial et al., 2022). However, the high levelized cost of electricity (LCOE) hinders the rapid developments of FWTs. One of the strategies to reduce the LCOE of FWTs is increasing the power generation of each wind turbine (Hofmann and Sperstad, 2014), which requires ever larger floaters. In this case, the structural flexibility of the floater and its consequences on global dynamic responses of FWTs become important. In the present work, the focus is on a semi-submersible FWT due to its wide application (Europe, 2017) in industry.

In most published research (Cao et al., 2021; Chen et al., 2017; Li et al., 2014, 2018; Wang et al., 2018), the flexibility of tower and rotor blades are taken into account in the simulations of FWTs, while the floater is considered as a rigid body assuming that the floater is much less flexible than other components. This assumption is invalid with the increasing size of wind turbine and floater (Moan et al., 2020). The further requirement for cost reduction may result in less material being used in floaters and implicitly more flexibility under environmental loads.

Some studies use different methods to consider the support structure's flexibility in the simulations of global dynamic responses of wind turbines. For monopile wind turbines, Sagar et al. (2015) conducted numerical co-simulations by coupling a full 3D finite-element model of the structure with flow simulations based on the Navier-Stokes equations and found that the flexible modes, especially the second mode, can increase the dynamic load remarkably. Similar conclusions can be found in the research of Suja-Thauvin et al. (2017) which considered the first and second flexible modes of a monopile. This finding is also observed in model tests (Suja-Thauvin et al., 2018) which tuned the first mode shape and first and second eigenfrequencies to fit those of the full-scale wind turbine by changing the material, length and thickness of the monopile. Borg et al. (2017, 2016) proposed a method to consider the spar-buoy flexibility within aero-hydro-servo-elastic simulation tools, including

* Corresponding author. School of Naval Architecture, Ocean and Civil Engineering, Shanghai Jiao Tong University, Shanghai, 200240, China.
E-mail address: zhengaosjtu@sjtu.edu.cn (Z. Gao).

https://doi.org/10.1016/j.oceaneng.2023.115584
Received 14 May 2023; Received in revised form 6 August 2023; Accepted 7 August 2023

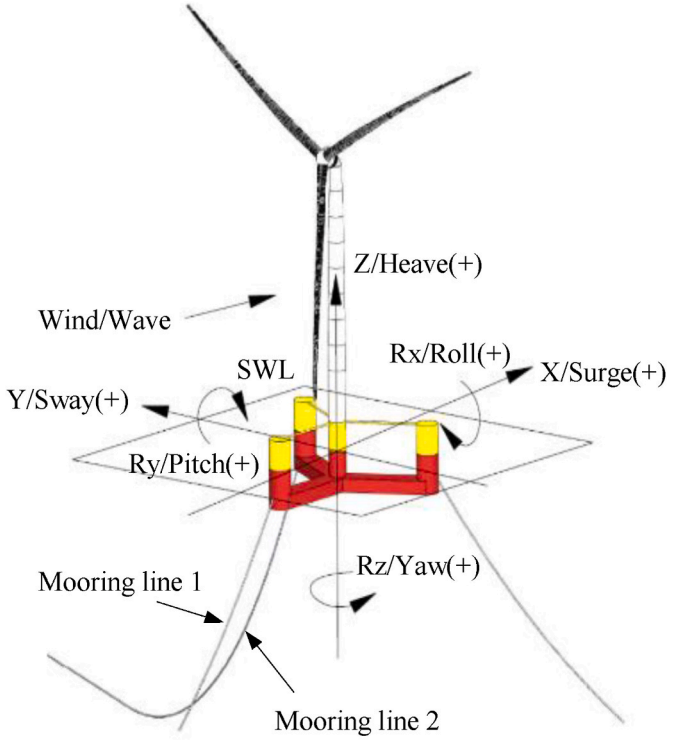

Fig. 1. Reference coordinate system for the 15-MW semi-submersible floating wind turbine system(Allen et al., 2020).

Table 1
Main properties of the wind turbine system (Allen et al., 2020).

Parameter	Unit	Value
Turbine Rating	MW	15
Rated Wind Speed	m/s	10.59
Maximum Rotor Speed	rpm	7.56
Hub Height (from the tower base)	m	150
Platform Type	-	Semi-submersible
Freeboard	m	15
Draft	m	20
Total System Mass	ton	20 093
Platform Mass	ton	17 839
Tower Mass	ton	1263
RNA(Rotor Nacelle Assembly) Mass	ton	991
Water Depth	m	200
Mooring System	-	Three-line chain catenary

wave-structure interactions based on linear radiation-diffraction theory. The spar-buoy flexibility had minor effect on the motion of wind turbine, but the first bending mode of the spar-buoy was coupled with pitch motion, indicating that the sectional loads of spar-buoy can be dependent on such motion. When designing a braceless semi-submersible FWT, Luan et al. (2016, 2017a) used a sectional approach where the hydrodynamic loads calculated from the linear potential flow theory were distributed over a beam model of the floater to derive the sectional loads. The results were further compared to the results from a frequency-domain model and validated against model tests (Luan et al., 2017b). A similar method was used in the simulations of TLP wind turbine (Souza and Bachynski, 2018) and found that the floater flexibility resulted in amplified heave and pitch responses, but the tower base load responses were not greatly influenced by flexibility in the pontoons. Henderson et al. (2010) performed a full coupled analysis for a TLP wind turbine within inclusion of modal deflections of support structure, observing that the heave and pitch natural frequencies differ from the results those from analysis with a rigid structure. The same conclusion was found by Zhao et al. (2012). In model tests of a multi-column FWT, Takata et al. (2021) used beams with a stainless steel core to obtain elastic similarity and urethane pieces to define the geometry. The results illustrated that the dynamic elastic deformations of the column affect the heave responses of the wind turbine.

The intended contribution of this paper is to describe a methodology that includes the modelling of flexible floaters in combination with coupled time-domain simulations and to investigate the effect of floater flexibility on the global dynamic responses for a 15-MW semi-submersible FWT, which is the four-column UMaine semi-submersible supporting the IEA 15-MW turbine (Allen et al., 2020). That is one objective of the EMULF (Efficient Modelling of Ultra Large Floating turbine) project funded by the COWI Foundation. First, the central column of the floater is modelled by multiple rigid bodies connected by flexible beams, while the remaining components of the floater are considered as one body. The first-order wave force transfer functions and frequency-dependent added mass and damping for each body are calculated based on the first-order potential flow theory. However, the quadratic transfer functions (QTFs) for the difference-frequency wave loads are estimated for the whole floater. The first order hydrodynamic loads are applied in the center of each beam. Then the flexible floater model is integrated in the numerical model of the FWT by connecting the beam elements of the floater with the elements of tower and mooring lines. The models with a flexible floater and a rigid floater are compared to analyze the effect of floater flexibility in terms of global dynamic responses under different environment conditions.

The organization of this paper is as follows. Section 2 briefly describes the properties of a 15-MW semi-submersible FWT. The methodology of modelling a flexible floater is presented in Section 3 together with the introduction of numerical tools. The global dynamic responses of the wind turbine, such as floater motions, tower base loads and mooring line tensions, from the models with a flexible and rigid floater are compared in Section 4. Conclusions are drawn in Section 5.

2. Properties of the IEA 15 MW wind turbine and the UMaine semi-submersible

To reduce the overall cost of floating wind turbines, the size of wind turbines and supporting structures is increasing. Even though time-domain coupled numerical tools have been developed and widely used to represent the complex behavior, tools and methodology are still missing to efficiently design and engineer floating wind turbine structures. Therefore, the objectives of the EMULF project are: (1) to develop numerical methods for global coupled aerodynamic/hydrodynamic loads and response analysis, focusing on future ultra-large floating wind turbines and accounting for floater flexibility; (2) to establish an advanced approach for structural stress analysis of floating wind turbine foundations following global time-domain analysis to close the gap between global response analysis and structural stress assessment for detailed structural design check; and (3) to develop a more efficient and cost-effective design methodology for conceptual design with focus on simplified frequency-domain and uncoupled approach and validation against fully coupled time domain approach. This work focuses on the first objective.

In the present work, the full wind turbine system consists of the IEA 15-MW reference wind turbine (Gaertner et al., 2020) and the UMaine VolturnUS-S reference semi-submersible platform (Allen et al., 2020), which is shown in Fig. 1 together with the reference coordinate system for the wind turbine system. The origin of the reference coordinate system is at the center of the central column at the mean sea level (MSL). The Z-axis points upwards, X-axis points from the upwind side column to the central column, and the Y-axis follows the right-hand rule. Table 1 shows the main properties of the full wind turbine system. The IEA 15-MW reference turbine is a Class IB 3-bladed direct-drive offshore wind turbine. It has a rotor diameter of 240 m and a hub height of 150 m. The key parameters of the turbine can be found in the IEA report (Gaertner et al., 2020).

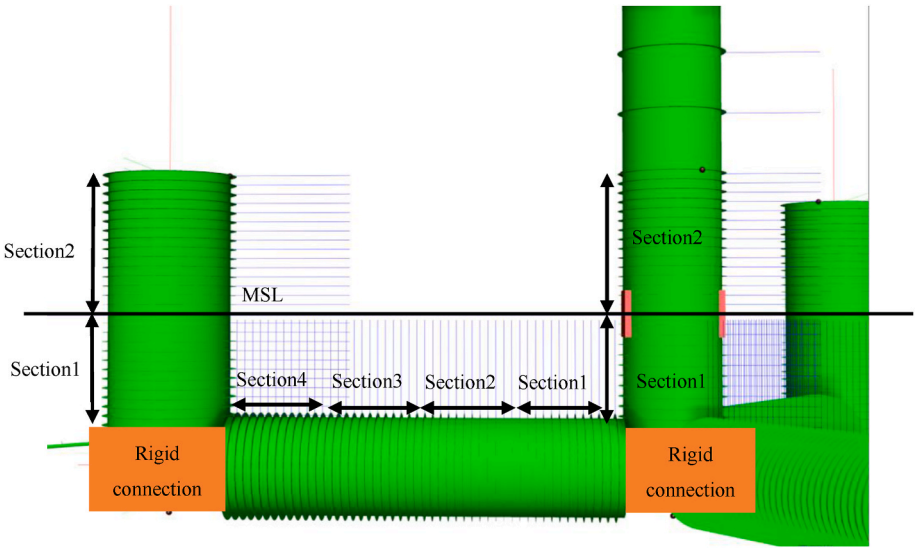

Fig. 2. The flexible floater sections for preliminary structural design.

Table 2
Comparison of natural frequency from free decay simulations.

Degree of freedom (DOF)	Rigid floater (Benchmark)	Flexible floater	Difference
	(Hz)	(Hz)	(%)
Surge	0.0074	0.0074	0.00
Sway	0.0073	0.0074	1.37
Heave	0.0485	0.0484	0.21
Roll	0.0350	0.0348	0.57
Pitch	0.0350	0.0347	0.86
Yaw	0.0110	0.0113	2.73

Table 3
Section properties of central column.

Parameter	Units	Section 1	Section 2
Length	m	13.00	15.00
Outer Diameter	m	10.00	10.00
Thickness	m	0.090	0.085
Mass per length	kg/m	23 343	22 244
Section area	m^2	2.802	2.648
Area moment of inertia	m^4	34.400	32.538
Radii of gyration	m	4.955	4.958

UMaine VolturnUS-S reference platform is a four-column steel semi-submersible platform. As shown in Fig. 1, the arrangement of the platform consists of three radially spaced buoyant vertical columns. At the center of the platform is the fourth buoyant column which connects the platform with the tower. This central column is connected to the outer columns through three rectangular pontoons and three struts attached to the bottom and top of the buoyant columns, respectively. However, the struts are not considered in the present study. The fixed iron-ore-concrete ballast is divided equally and placed at the base of the three radial columns. Seawater ballast floods the majority of three submerged pontoons, and is considered as fixed in the present numerical simulations.

2.1. Preliminary structural design of the floater

The VolturnUS-S reference semi-submersible platform does not have publicly available structural properties of the floater. Therefore, for the investigation of the effect of floater flexibility, COWI generated a preliminary structural design of the floater in the EMULF project.

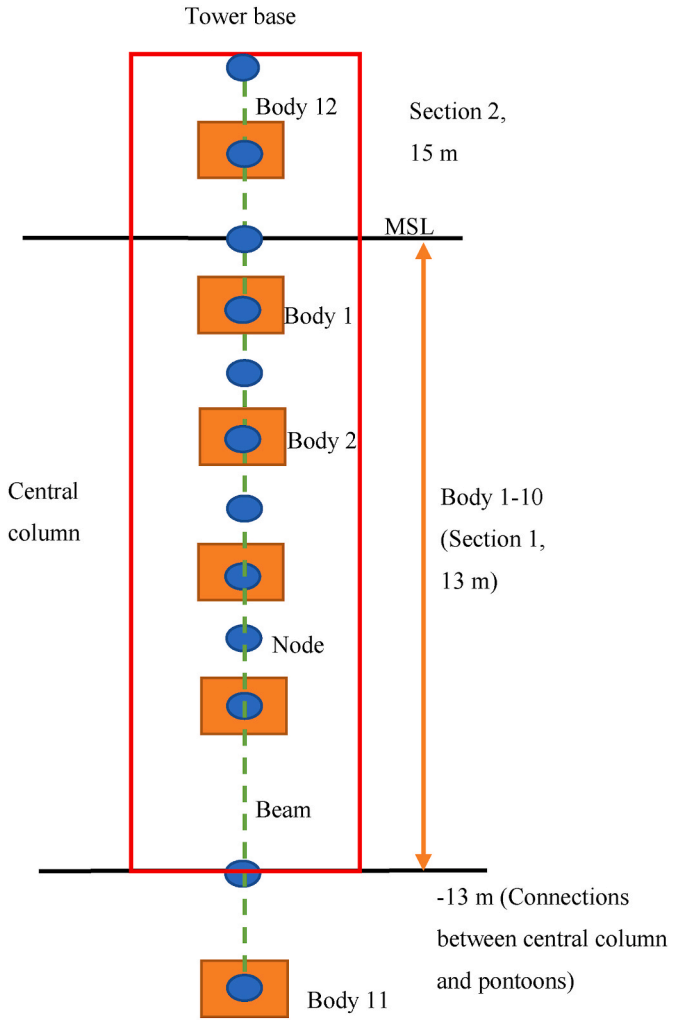

Fig. 3. Definition of a finite element model of the central column of the floater.

In the initial design process, the floater is built by beam elements to extract the cross-sectional forces. The hydrodynamic loads on each beam

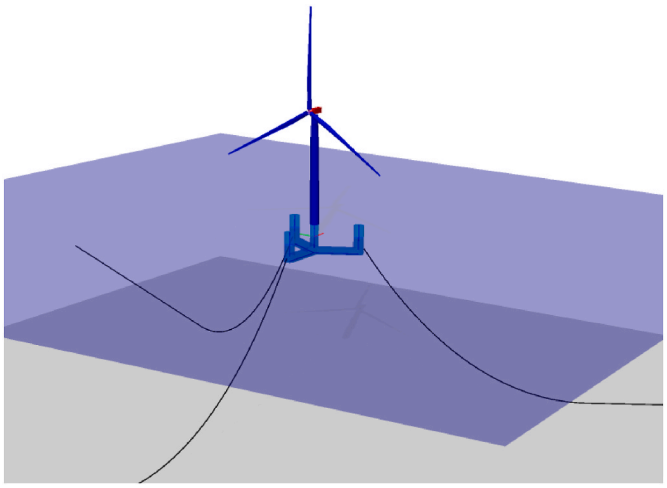

Fig. 4. The 15-MW semi-submersible FWT model in SIMA.

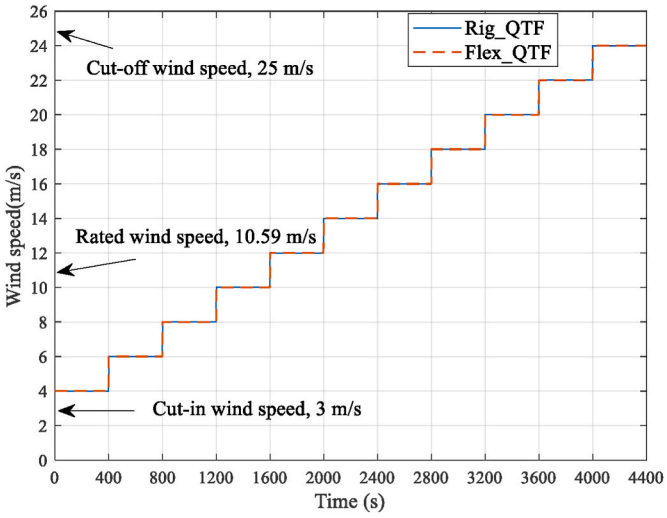

Fig. 5. Wind speed for a wind ramp condition (LC1).

Table 4
Overview of different numerical models in SIMA.

Label	Rigid floater	Flexible floater	Include difference-frequency wave force
Rigid_Lin	✓	×	×
Rigid_QTF	✓	×	✓
Flex_Lin	×	✓	×
Flex_QTF		✓	✓

Table 5
Definition of load cases 3 and 4 (LC3 and LC4).

Label	Irregular wave		Turbulent wind	
	Significant wave height (m)	Spectral peak period (s)	Mean wind speed (m/s)	Turbulence intensity (-)
LC3-1	1.10	4.60	-	-
LC3-2	3.62	8.52	-	-
LC3-3	10.70	14.20	-	-
LC4-1	1.18	4.76	6	0.21
LC4-2	1.84	5.88	12	0.15
LC4-3	3.62	8.71	20	0.12

are calculated based on Morison's equation for this initial sizing process. The rectangular pontoons are simplified as cylindrical pontoons (Fig. 2). This simplification is only used for the estimation of the cross-sectional forces during initial design. The added mass and drag coefficients of the flexible floater beams are tuned by matching the free decay results from the simulation of the flexible floater model with a rigid floater model as a benchmark. The drag coefficients of the simplified cylindrical pontoons are also used in the simulations of flexible floater model in Section 3. The comparisons of natural frequencies calculated from free decay simulations are found in Table 2. The differences are relative to the results of rigid floater.

The results from the numerical simulations are post-processed to take out the maximum bending moment and contemporary loads at several locations along each cross-section on the floater. The maximum loads at each location under different environment conditions which are defined by the IEC 61400-3 standard (Commission, 2009) are used for design.

Based on the obtained loads, the floater is designed with stiffened plates for the pontoon and ring-stiffened cylinders for the columns. The connections between pontoons and columns are assumed to be stiffer than the corresponding element stiffness. These connections are modelled as rigid bodies and no detailed design is carried out. The stress calculation considers normal, transverse and shear stresses in the plates, as well as hydrostatic pressure. The hydrostatic pressure is considered by adding up static and dynamic contributions (due to wave elevation) for each element according to DNVGL-OS-C103 (DNV, 2018). The floater is divided into several sections which use the same cross section. The pontoons have four sections while the center column and outer columns use two sections, shown in Fig. 2. For each section on the columns and pontoon, normal and shear stresses are calculated at several key points. The normal stress is calculated from axial force and bending moments, and the shear stress is found from shear force and torsion. The calculated stresses are then used for the design check of the section. This is an iterative process between satisfying the design checks and minimizing weight.

The design criteria for the columns are defined from DNV-RP-C202 (Veritas, 2010) and the software CYLSHELL is used for the design checks. The software STIPLA-DNVRP is used to check the design of pontoons where the plate and stiffener are checked based on the DNV-RP-C201(Lloyd, 2010), DNV-OS-C101 (DNV, 2016) and DNV-OS-C201 (DNV, 2017). In the current work, only the central column is considered to be flexible. This is because the connection between the central column and the pontoons is typically designed to have much higher stiffness so that it is only the central column that will influence the natural period and shape of the first tower bending mode, under the wind excitations. However, the same modeling approach can be used when the other parts of the floater need to be modelled as flexible. The section properties of the central column are given in Table 3.

3. Methodology

3.1. Structural modelling of a flexible floater

In the proposed methodology of modelling a flexible floater, the central column between tower base and the connection with pontoon (13 m below MSL) is considered as an assembly of several rigid bodies (Body 1–10 and Body 12 in Fig. 3) while the remaining components of the floater are considered as one rigid body (Body 11 in Fig. 3). A beam finite element model can then be developed in the global coordinate system. The properties of Section 1 (Table 3) are applied in the beams between Body 1 and 11 while the properties of Section 2 (Table 3) are used in the beam between Body 1 and Body 12. Each rigid body is attached to a node which has 6 degrees of freedom (DOFs). Each beam is

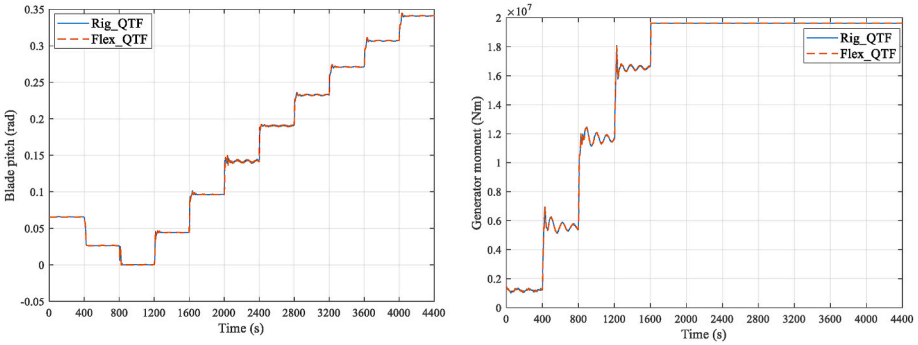

Fig. 6. Time series of blade pitch angle (left) and generator moment (right) under wind ramp condition.

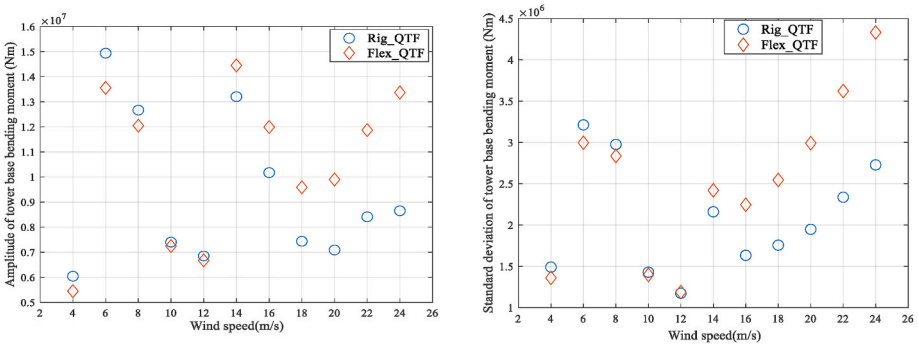

Fig. 7. Amplitude (left) and standard deviation (right) of tower base bending moment under wind ramp condition.

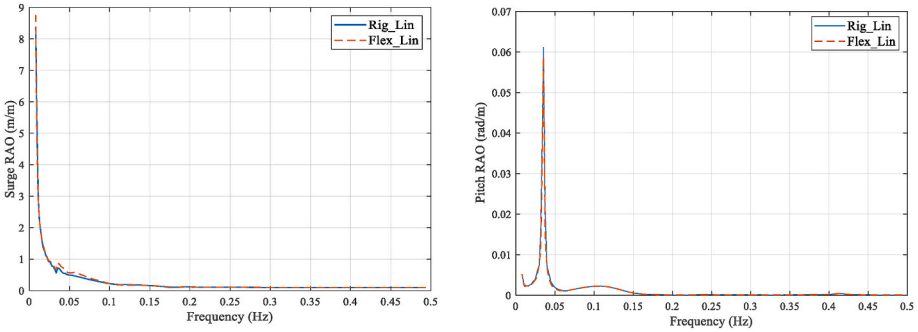

Fig. 8. RAO of surge (left) and pitch (right) under regular wave condition.

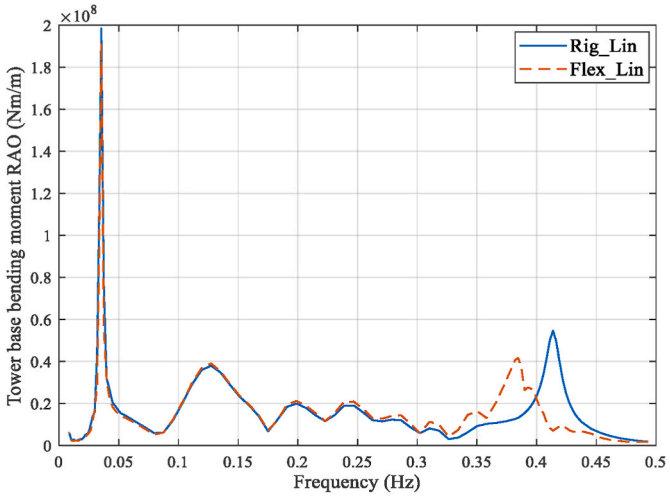

Fig. 9. RAO of tower base bending moment under regular wave condition.

divided into 10 elements. The inertia loads, the gravity loads, and the hydrostatic and hydrodynamic loads of each body are calculated and transferred to the node that corresponds to the body in the finite element model. The hydrostatic and hydrodynamic loads on each body are estimated by integrating the hydrostatic and hydrodynamic pressure on the wet surface of the body. The pressures are usually obtained through a frequency-domain analysis using a panel method which is more valid than Morison's equation for large-volume structures of floating wind turbines. The global dynamic responses and loads in each body of the floater can be obtained by conducting a time-domain finite element analysis and extracting results at the nodes.

The time-domain analysis is performed using the software SIMA (SIMO (MARINTEK, 2012)-RIFLEX (Ormberg and Passano, 2012)), developed by SINTEF Ocean and widely validated in the analyses of numerous of offshore wind turbines. In general, the hydrodynamic loads on bodies are considered in SIMO while the system is modelled using beam and bar elements based on small strain theory in the non-linear finite element solver RIFLEX.

In SIMA, the blades are modelled using flexible beam elements with

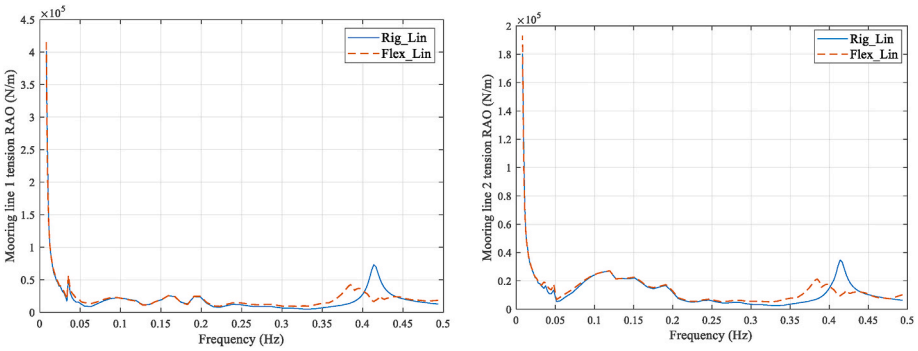

Fig. 10. RAO of mooring line 1 tension (left) and mooring line 2 tension (right) under regular wave condition.

two planes of symmetry to differentiate the flapwise and edgewise stiffness. The tower and shaft are modelled using axisymmetric beam elements. The hub and nacelle are modelled as rigid bodies with corresponding structural mass and inertia. The tower is connected to the rotating shaft through a flexible joint. The electric torque from the generator is applied at this joint to regulate the rotational speed according to the prescribed control strategy. The Reference OpenSource Controller (ROSCO) (Abbas et al., 2020; Laboratory, 2019) from National Renewable Energy Laboratory (NREL) is used in the current work. In below-rated wind speeds, the wind turbine operates at the optimal tip speed ratio with a proportional integral controller to regulate the generator moment. In above-rated wind speed, the blade pitch controller

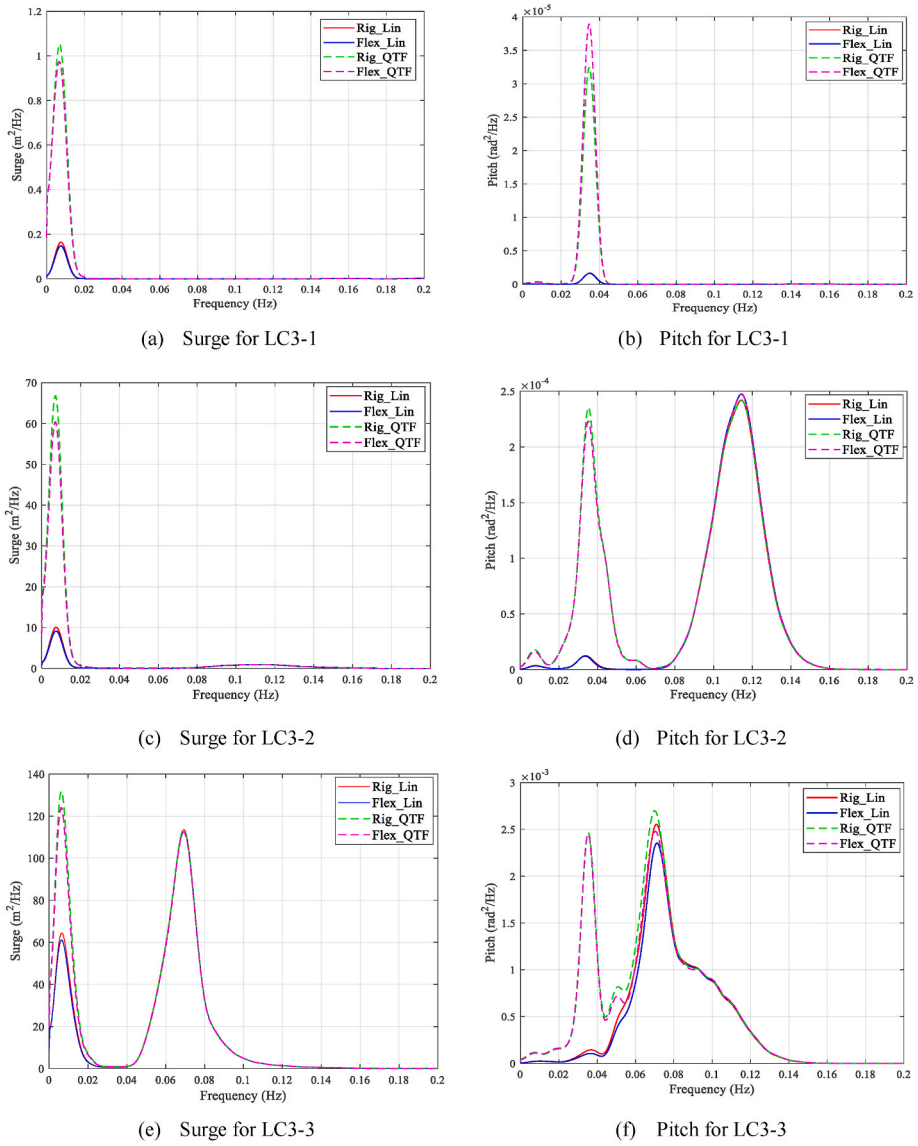

Fig. 11. Spectra of surge and pitch motions under irregular wave conditions.

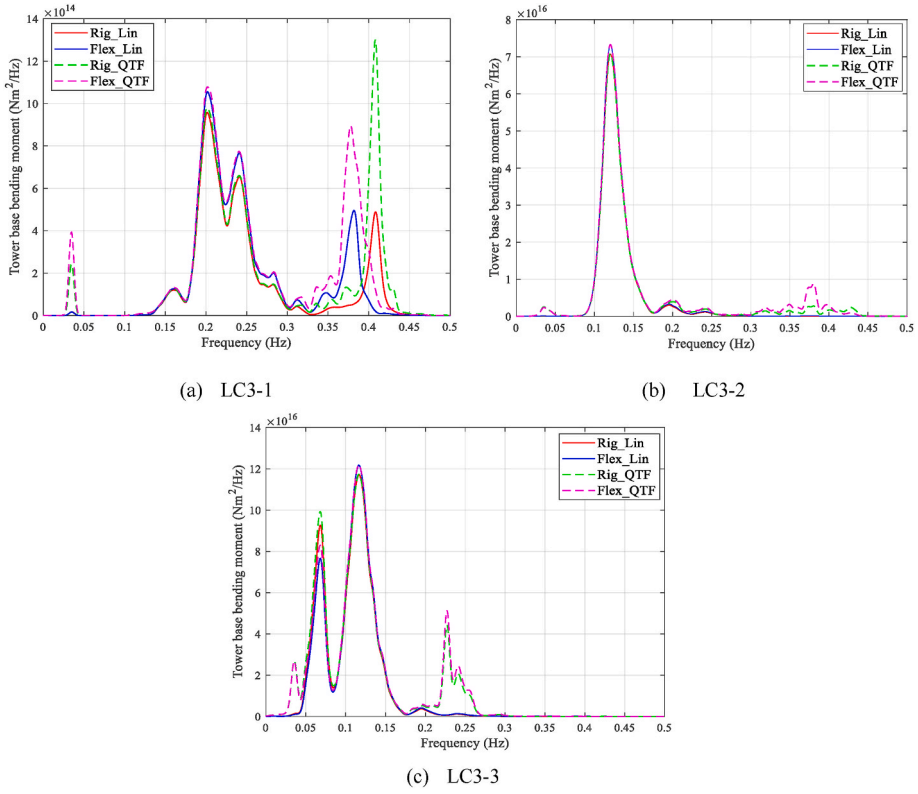

Fig. 12. Spectra of tower base bending moments under irregular wave conditions.

is used to achieve the constant-power and constant-speed output. The mooring lines are modelled as nonlinear bar elements: only the axial stiffness is considered, while torsional and bending stiffness are neglected. Hydrodynamic loads on the mooring lines are included using Morison elements with both the added mass and drag terms. The beams at the tower base and the top of central column use the same node so that the flexible floater is linked with the tower. Master-slave connections are applied to integrate the motions between the flexible floater and fairleads of mooring lines. A graphical illustration of the semi-submersible FWT in SIMA is shown in Fig. 4.

3.2. Hydrodynamic modelling of a flexible floater

In SIMA, the motions of each rigid body can be represented as:

$$[\mathbf{M}_i + \mathbf{A}_i(\infty)]\ddot{\mathbf{x}}_i(\mathrm{t}) + \int_{-\infty}^{\infty} \boldsymbol{K}_i(\mathrm{t}-\tau)\dot{\mathbf{x}}_i(\tau)\mathrm{d}\tau + \mathbf{C}_i\mathbf{x}_i(t) = \mathbf{F}_i^{(1)} + \mathbf{F}_i^{(2)} + \mathbf{F}_i^{(D)} + \mathbf{F}_i^{(R)} \quad (1)$$

where i is the index of each body, $\mathbf{M}$ is the 6×6 mass matrix of each body, $\mathbf{A}(\infty)$ is the 6×6 infinite-frequency added mass matrix, $\ddot{\mathbf{x}}$, $\dot{\mathbf{x}}$, and $\mathbf{x}$ are the 6×1 acceleration, velocity and displacement vectors of each body, respectively. $\mathbf{K}(\mathrm{t}-\tau)$ is the retardation function which represents the fluid memory and is calculated from the frequency-dependent potential damping. $\mathbf{C}$ is the 6×6 hydrostatic restoring matrix, $\mathbf{F}^{(1)}$ and $\mathbf{F}^{(2)}$ are the first-order and second-order wave excitation forces and moments, respectively, calculated based on the wave force transfer functions. $\mathbf{F}^{(\mathrm{D})}$ is Morison drag force and $\mathbf{F}^{(\mathrm{R})}$ are the cross-sectional forces acting on the body through the connected flexible beam elements. In order to obtain the hydrodynamic coefficients of each body, i.e. the frequency-dependent potential damping, added mass coefficients and wave force transfer functions, the potential-flow boundary value problem must be solved by assuming the whole floater is a rigid body in the global coordinate system shown in Fig. 1. The hydrodynamic interaction between multiple bodies is considered, under the assumption of constrained motions. Each body follows the global floater motions in the solution of the potential-flow boundary value problem. The pressure on the wet surface of the floater is calculated based on the velocity potential and Bernoulli's equation. Integration of all the pressure on each corresponding rigid body is needed to obtain the resultant forces and moments acting on each body which are used to derive the hydrostatic and hydrodynamic coefficients.

There are four assumptions in the present work in the derivation of hydrostatic and hydrodynamic coefficients for each body:

1) The seawater ballast inside the floater is considered as ballast mass which applies inertia loads on the floater instead of the hydrostatic pressure on the corresponding inner surface of the floater.
2) Hydroelasticity effects are not considered. Essentially, it is assumed that the deformation due to floater flexibility is very small as compared to the rigid-body motions, and therefore the hydrostatic/hydrodynamic loads are not influenced by floater flexibility.
3) Second-order hydrodynamic pressures on each panel are assumed to be small (from the local effect point of view) and therefore lumped to the remaining components of the floater (Body 11 in Fig. 3). The second-order hydrodynamic loads considered here are only the difference-frequency wave loads which need be considered in the global dynamic response analysis.
4) Viscous effects are modelled as drag forces on each body for the global dynamic response analysis.

Details of the approaches to derive the hydrostatic and hydrodynamic coefficients of each body of floater follow the WAMIT theory manual (Lee, 1995) and the PhD thesis of Chenyu Luan (2018), and are briefly illustrated as follow.

In the linear potential flow theory, the equations for the added mass (A_{ij}) and damping coefficients (B_{ij}) and first-order wave excitation force (X_i) of each body can be represented as:

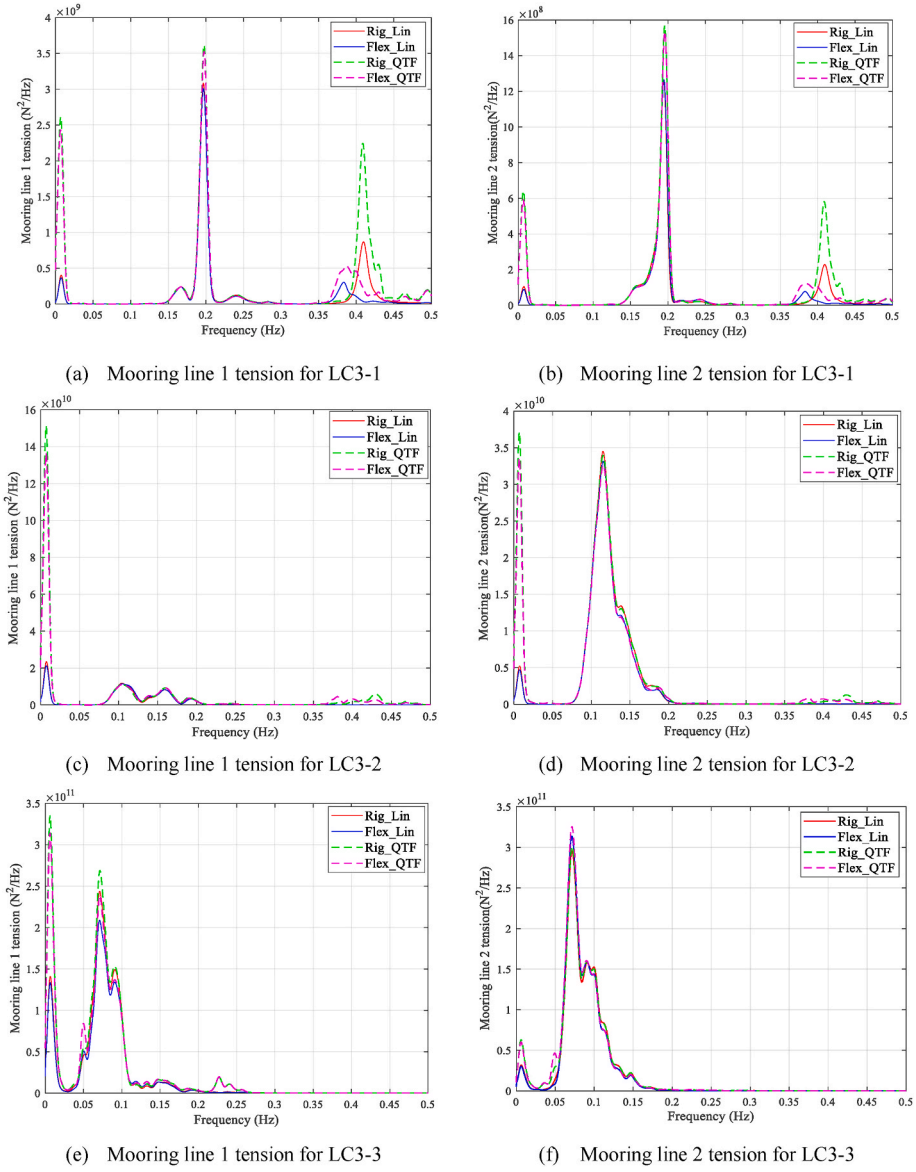

Fig. 13. Spectra of mooring line tensions under irregular wave conditions.

$$A_{ij} - \frac{i}{\omega}B_{ij} = \rho \iint_S n_i \varphi_j dS \tag{2}$$

$$X_i = -i\omega\rho \iint_S n_i \varphi_D dS = - - i\omega\rho \iint_S \left(n_i \varphi_0 - \varphi_i \frac{\partial \varphi_o}{\partial n}\right) dS \tag{3}$$

where i, j are the DOFs for body motions, ρ is the fluid density, n is the generalized normal vector of the body surface, ω is the incident wave frequency, S is the instantaneous wet surface of the body, φ_0 is the incident wave velocity potential, φ_D is the diffracted wave velocity potential and φ is the radiated wave velocity potential. Therefore, the challenge is to obtain the generalized normal vector of body surface and velocity potential for each panel of each body. The specific steps are: 1) solving the boundary value problem in the global coordinate system with the rigid-body assumption for the whole floater in WAMIT, 2) distributing the results (generalized normal vector and velocity potential) of all the panel to the corresponding body based on the coordinate of each panel, 3) integrating the velocity potential along the wet surface of each body to obtain the resultant first-order wave excitation force, added mass and damping, and 4) deriving the hydrodynamic coefficients in the global coordinate system based on the results of step 3.

The linear hydrostatic restoring force (F_i) of each body can be represented as:

$$F_i = -\rho g \iint_{S-S_0} z n_i dS = C_{ij} \bullet \eta_j \tag{4}$$

where i, j are the DOFs for body motions, ρ is the fluid density, S is the instantaneous wet surface of the body, S_0 is the mean position of the body surface, z is the vertical coordinate of each panel of body, n is the generalized normal vector of the body surface, C_{ij} is the 6×6 hydrostatic restoring matrix, η_j represents the motions of each body in the global coordinate system and is a 6×1 vector. The hydrostatic restoring matrix is obtained by the following steps, 1) distributing the generalized normal vector and vertical coordinate of each panel to the corresponding body based on the coordinate of each panel, 2) integrating the linear hydrostatic pressure ($-\rho g z$) along the wet surface of each body to obtain the linear hydrostatic restoring force in the global coordinate system, and 3) the hydrostatic restoring matrix is calculated by setting the motion of body (η_j) to be an unit vector in each DOF based on Eq. (4). Through this method, the calculated restoring matrix refers to the global coordinate system and only includes the contribution of hydrostatic

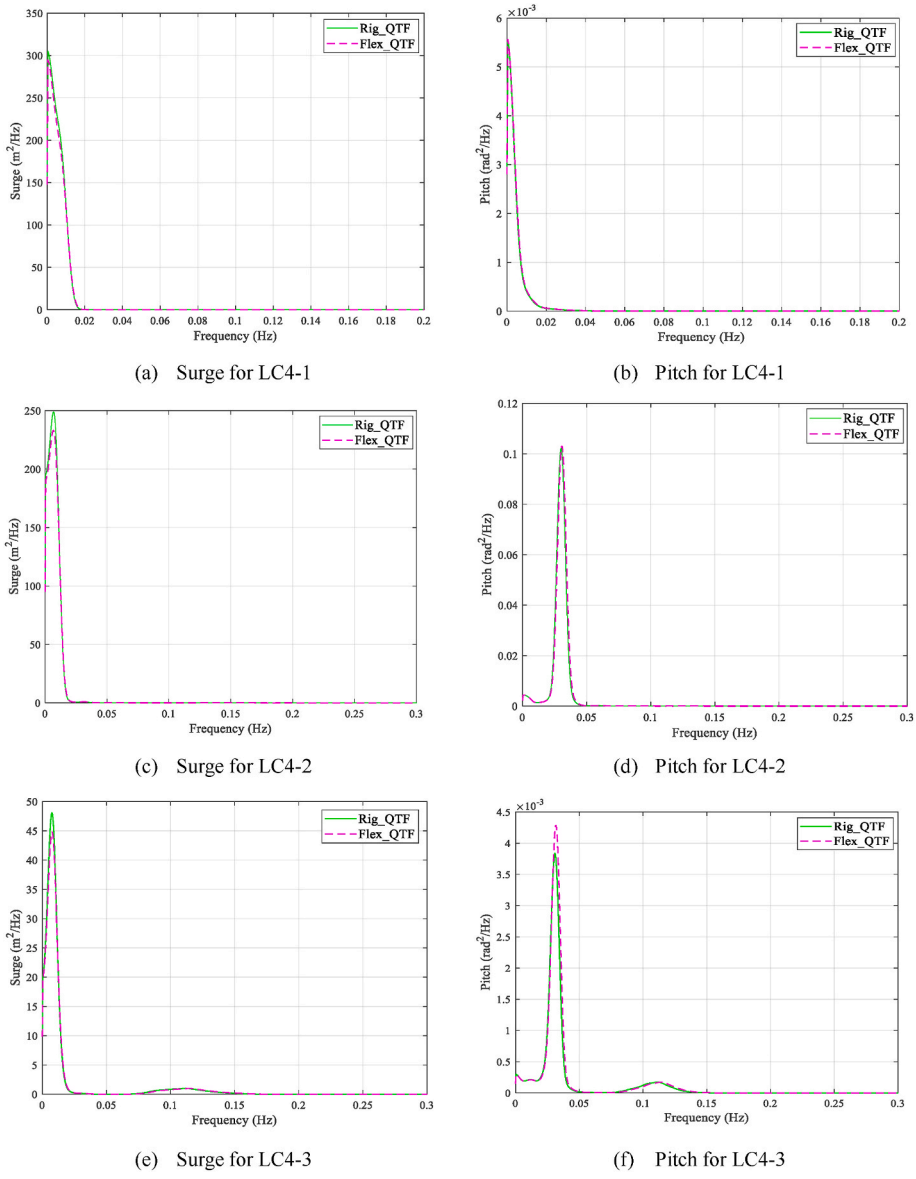

Fig. 14. Spectra of surge and pitch motions under irregular wave and turbulent wind conditions.

pressure, without the contribution of gravity loads. Hence, the gravity load for each body will be explicitly applied at the center of gravity, always downward, moving with the center of gravity in the static and dynamic analysis. This can model the contribution of the gravity to the restoring effect. To ensure the equilibrium of the whole floater at rest, the 6-DOF buoyancy force from the hydrostatic equilibrium condition should be explicitly applied. It is applied at the coordinate system origin, always upward, moving with the coordinate system origin. That means this force will not contribute to the restoring effect.

Second-order potential flow theory is applied to account for the difference-frequency wave loads with assumption of a rigid-body for the whole floater. The QTFs obtained from WADAM (MANUAL, 2017) are used to calculate the difference-frequency wave loads in the time--domain analysis of SIMA. Viscous effects are taken into account by applying the drag term of Morison's equation on each body of the floater. The drag coefficients are determined by the data used in the preliminary structural design of the floater in Section 2.1.

3.3. Numerical model

To investigate the effect of floater flexibility, a numerical model with a rigid floater is also built in SIMA for comparison. All the parameters for these two floaters are same except for the structural model of the central column. The rigid floater is represented as one rigid body in SIMA while the flexible floater is built by multiple rigid bodies connected by flexible beams following the methodology discussed in Section 3.1 and 3.2. In addition, each numerical model is run with and without the second-order difference-frequency wave forces. Detailed descriptions for the numerical models are available in Table 4.

3.4. Load cases

Four main load cases are defined to investigate the effect of floater flexibility on the global dynamic responses of wind turbine.

Load case 1 (LC1) is defined by the wind ramp. The wind speed starts at 4 m/s and ends at 24 m/s with steps of 2 m/s, and each wind speed is maintained for 400 s, as shown in Fig. 5 together with the cut-in, rated and cut-out wind speed of wind turbine. The wind direction is along the positive x direction of global coordinate system. This load case can also validate whether the prescribed control strategy in SIMA works normally.

Load case 2 (LC2) is given as a series of regular waves without wind,

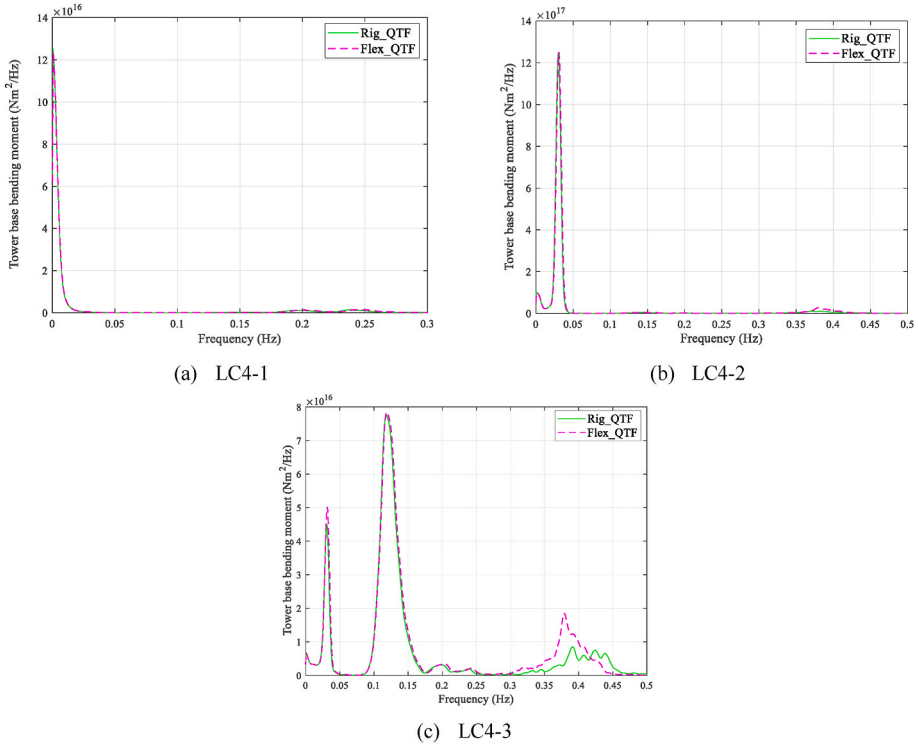

Fig. 15. Spectra of tower base bending moments under irregular wave and turbulent wind conditions.

propagating along the positive x direction of the global coordinate system. The wave height is set to 1 m while the wave frequency varies from 0.01 Hz to 0.5 Hz with a varying step.

Load case 3 (LC3) is defined as a series of irregular wave without wind and load case 4 (LC4) is defined as the combination of irregular waves and turbulent wind, and described in Table 5. The irregular wave is generated based on the JONSWAP spectrum with the peak enhancement factor equal to 2.5. The turbulent wind is built based on the Kaimal spectrum and exponential coherence model and the corresponding turbulence intensity is shown in Table 5. The wave also propagates along the positive x direction of the global coordinate system.

4. Results and discussions

In this section, the results of the simulations are presented and discussed for the four main load cases defined in Section 3.4. The variations in the numerical model are used to investigate the effect of floater flexibility on global dynamic responses of a 15-MW semi-submersible wind turbine. The motion for the flexible floater refers to the motion of the body at the origin of coordinate system. Due to the symmetry of the floater, and the fact the wind and waves travel along an axis of symmetry (Fig. 1), the mooring line tension on the starboard side should be equal to the tension on the port side. Therefore, only the tension of upwind mooring line (mooring line 1, Fig. 1) and mooring line on the starboard side (mooring line 2, Fig. 1) are discussed in this section. The mooring line tension is calculated at the fairlead. Furthermore, the responses of the tower base shear force are qualitatively similar to the responses of tower base bending moment, so only the responses of tower base bending moment are presented in this section. The transient phase at the start of simulations is eliminated before post-processing. The power spectral density (PSD) of dynamic response for LC3 and LC4 is calculated based on 1-h simulation.

4.1. Wind ramp condition (LC1)

In this load condition, there is no incident wave, so the inclusion of the QTFs for the difference-frequency wave loads in the numerical models has no influence on the results. Therefore, only 'Rigid_QTF' and 'Flex_QTF' are compared.

The numerically estimated blade pitch angle and generator moment of rigid and flexible floater under wind ramp condition are compared in Fig. 6. The generator moment increases with wind speed in the below-rated wind speed. When wind speed is over the rated-wind speed, the generator moment is constant. Furthermore, there is a good agreement between the rigid and flexible floater model. As expected, the prescribed control strategy is not affected by the central column flexiblity.

By comparing the statistical results of motions and mooring line tensions for the rigid and flexible floater under the wind ramp condition, no significant difference can be observed between the models, which are not presented in the current work. The mean values of tower base bending moments are almost same between rigid and flexible floater, but the amplitude (maximum of the moment minus the minimum of the moment) and standard deviation show a significant difference, which are compared in Fig. 7. Below rated-wind speed, the rigid and flexible floater model predict similar amplitude and standard deviation of tower base bending moment. In above-rated wind speeds, the amplitude and standard deviation of tower base bending moment in the flexible floater model is over 20% larger than those in the rigid floater model.

In conclusion, the floater flexibility has no significant effect on the global dynamic responses of the wind turbine under only-wind condition, except for the tower base bending moments.

4.2. Regular wave conditions (LC2)

This sub-section assesses the effect of floater flexibility on the global dynamic responses of the wind turbine under regular wave conditions. All the numerical simulations are carried out without consideration of the QTF for the difference-frequency wave loads. Response amplitude operators (RAOs) of dynamic responses of the wind turbine are calculated based on 10 steady-state wave cycles.

Numerically calculated surge and pitch RAO for the rigid and flexible floater model are compared in Fig. 8. There is a good agreement across

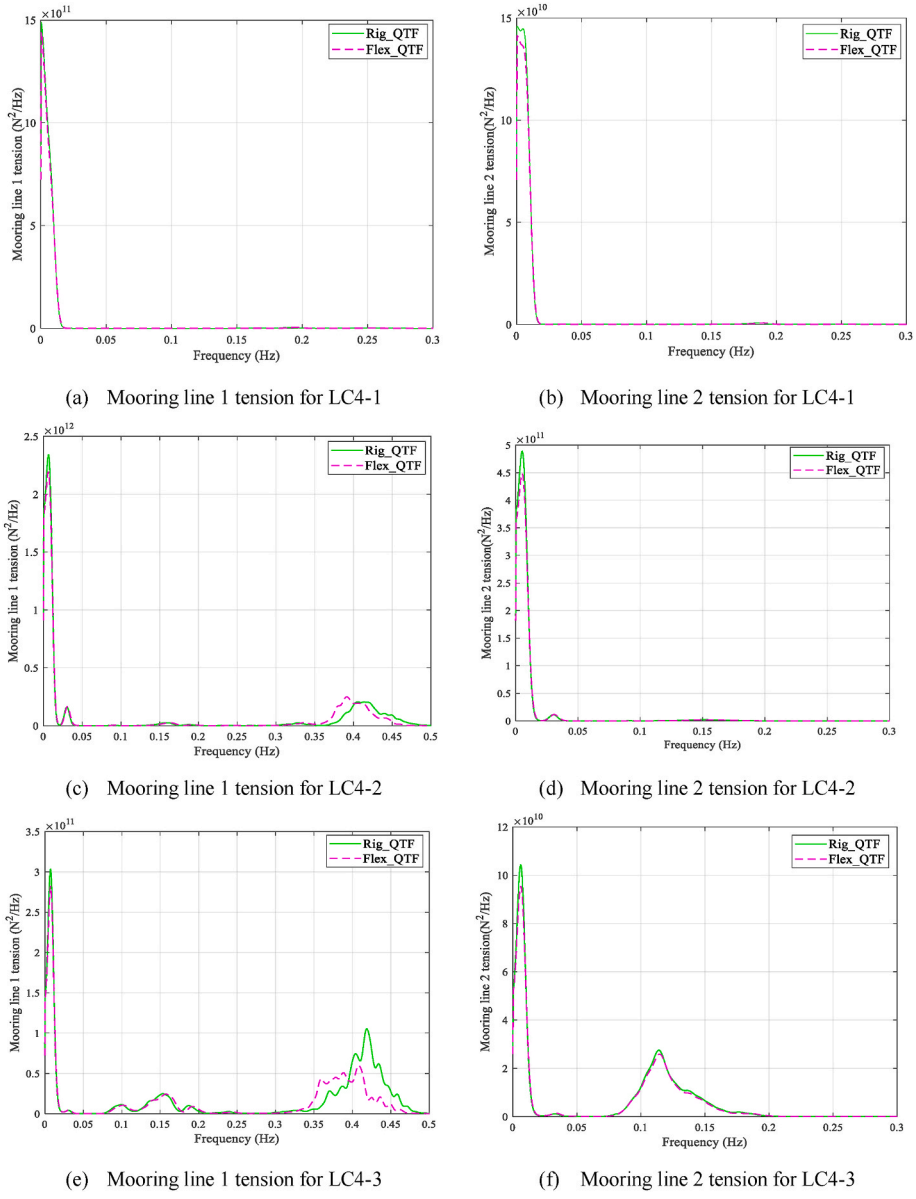

Fig. 16. Spectra of mooring line tensions under irregular wave and turbulent wind conditions.

all calculated wave frequencies except for small differences near the surge or pitch resonance. The effect of the central column flexibility on the motions of the wind turbine under regular wave condition is seen to be negligible.

Fig. 9 compares the RAOs of tower base bending moments under different wave frequencies. When the wave frequency is below 0.3 Hz, the tower base bending moment calculated from the flexible floater model agree well with those from the rigid floater model. However, the responses over 0.3 Hz show a significant difference. The tower bending natural frequency of flexible floater is reduced from 0.41 Hz for the rigid floater model to 0.38 Hz. Furthermore, the flexible floater model predicts smaller tower base bending moments around tower bending natural frequency compared to the responses in the rigid floater model. When the floater is modelled as flexible, it increases the structural damping in the floater and tower system, which gives a smaller amplitude.

The RAOs for the tension of upwind mooring line (mooring line 1) and mooring line on the starboard side (mooring line 2) are shown in Fig. 10. Similar to the RAOs of the tower base bending moments, no significant difference of the mooring line tensions below 0.3 Hz is found between rigid and flexible floater models. However, the results close to the tower bending natural frequency are changed similar to the change in the tower base bending moment response.

4.3. Irregular wave conditions (LC3)

In this sub-section, the effect of floater flexibility on global dynamic responses of the wind turbine under irregular wave conditions is investigated. At the same time, the numerical models with the difference-frequency QTFs are compared against the models without the difference-frequency QTFs to analyze the influence of the difference-frequency wave loads on the global dynamic responses of the wind turbine.

The numerically estimated surge and pitch motions under irregular wave conditions using different numerical models are compared in Fig. 11. In the mild wave condition (LC3-1), response at the surge resonance frequency (0.074 Hz) dominates surge motion and pitch resonance (0.036 Hz) dominates pitch motion. As the wave height increases, the contribution from wave-frequency response becomes more important. As previously shown in regular waves (LC2), the floater

flexibility has no effect on the rigid-body natural frequencies. The surge and pitch natural frequencies are outside the linear wave-excitation range, and can be excited by nonlinear wave loads. Therefore, the inclusions of QTF for the difference-frequency wave loads significantly increase the resonant response in surge and pitch (Rig_Lin vs Rig_QTF or Flex_Lin vs Flex_QTF in Fig. 11). The difference of responses in the low frequency or wave frequency range between rigid and flexible floater model are quite small except for the pitch motion in LC3-1. The reason can be related to the numerical error due to quite small pitch motion. The significant amplitude of pitch motion in LC3-1 is about 0.001 rad, less than one-tenth of significant amplitude in LC3-2 and one percent of significant amplitude in LC3-3.

Fig. 12 compares the tower base bending moments under irregular wave conditions. The PSD of tower base bending moments shows three distinct frequencies: the pitch natural frequency at 0.036 Hz, the linear wave excitation, and the tower bending natural frequency around 0.35–0.4 Hz. In the mild wave condition (LC3-1), the responses around wave frequency and tower bending natural frequency dominate, while the wave-frequency responses dominate in the moderate and severe wave condition (LC3-2 and LC3-3). As seen previously, the tower bending natural frequency in the flexible floater model reduces to 0.38 Hz compared to 0.41 Hz for the rigid floater model. Additionally, the numerical model with QTF predicts larger responses around the pitch natural frequency and tower bending natural frequency (Rig_Lin vs Rig_QTF or Flex_Lin vs Flex_QTF in Fig. 12), consistent with the larger motions in the numerical model with difference-frequency QTFs. Furthermore, the contribution of difference-frequency wave by difference-frequency QTFs to the wave-frequency responses is also observed, especially in the severe wave condition (LC3-3). The increased responses around the tower bending natural frequency and pitch natural frequency in the flexible model will increase the fatigue damage of tower base and extreme tower base bending moments, respectively.

The upwind mooring line (mooring line 1) tension and the tension of mooring line on the starboard side (mooring line 2) under irregular wave conditions are shown in Fig. 13. Response at the surge resonance frequency and wave frequency dominate the mooring line tension. Furthermore, in the mild wave condition (LC3-1), a smaller peak is observed at the tower bending natural frequency and the change of this natural frequency is also found between rigid and flexible floater model. The QTFs for the difference-frequency wave loads have the same effect on the mooring line tension as on floater motions and tower base bending moments, with increasing of responses around surge natural frequency and tower bending natural frequency. Meanwhile, the inclusion of the difference-frequency QTFs lead to larger mooring line tensions in the wave frequency range, which can be found in the results of LC3-1 and LC3-3 (Fig. 13 (a), (b) and (e)).

4.4. Irregular wave with turbulent wind conditions (LC4)

The effect of floater flexibility on the global dynamic responses of the wind turbine under irregular wave and turbulent wind conditions are discussed in this sub-section. All the numerical models are simulated with consideration of the QTF for the difference-frequency wave loads.

The numerically calculated surge and pitch motions of flexible floater model are compared against the results of rigid floater model under irregular wave and turbulent wind conditions in Fig. 14. At the lower mean wind speed (LC4-1), the surge and pitch motion are mainly affected by the wind and the responses occurs in the wind frequency. The contributions from the wave frequency or the tower bending natural frequency to the surge or pitch motion are negligible. At higher mean wind speeds (LC4-2 and LC4-3), the response at the surge resonance frequency dominates surge motion and pitch resonance frequency dominates pitch motion. In addition, the rigid floater and flexible floater model predict similar surge and pitch responses which illustrates that the floater flexibility has no significant influence on the motion of the wind turbine under irregular wave and turbulent wind conditions.

The tower base bending moments under irregular wave and turbulent wind conditions are shown in Fig. 15. In below-rated wind speed condition (LC4-1 and LC4-2), the largest contribution to the tower base bending moments comes from the low-frequency components, such as wind frequency component for LC4-1 and pitch natural frequency component for LC4-2. In the above-rated wind speed condition (LC4-3), the PSD of tower base bending moment shows three distinct frequencies: the pitch natural frequency, the linear wave excitation and the tower bending natural frequency. The floater flexibility has minor effect on the low-frequency and wave frequency tower base bending moments, which can be demonstrated by small difference of responses in the low-frequency and wave frequency region. However, the floater flexibility changes the tower bending natural frequency and increase the responses around the tower bending natural frequency. The blade passing frequency (3 P) is around 0.37 Hz, close to the tower bending natural frequency (0.38 Hz) for the flexible model. Therefore, the more excitations are applied in the flexible model and increase the responses around the tower bending natural frequency.

Fig. 16 compares the upwind mooring line (Mooring line 1) tension and the tension of mooring line on the starboard side (Mooring line 2) under irregular wave and turbulent wind conditions. It can be found the main contribution for the mooring line tension, similar to the surge motion, comes from the wind frequency (LC4-1) or the surge natural frequency (LC4-2 and LC4-3). At the higher mean wind speeds (LC4-2 and LC4-3), there is a peak around tower bending natural frequency for the upwind mooring line tension (Fig. 16 (c) and (e)). The variation of the tower bending natural frequency influenced by the floater flexibility can be observed. The mooring line tension has a wave-frequency response in above-rated wind speed (Fig. 16 (e) and (f)). Furthermore, the floater flexibility has a significant influence on the mooring line tension at the tower bending natural frequency and a minor effect on the tensions in the low-frequency and wave frequency range.

5. Conclusions

This study investigates the effect of floater flexibility on global dynamic responses of an ultra-large semi-submersible floating wind turbine. The focus is on the responses under the constant wind, regular wave, irregular wave, and irregular wave with turbulent wind conditions.

In the conventional time domain analysis for the wind turbines, the floater is considered as a rigid body. Therefore, a methodology of modelling a flexible floater in a time domain code is firstly proposed in the current work. In the proposed methodology, the central column of the floater is considered as an assembly of several rigid bodies while the remaining components of floater are considered as one rigid body. Each body is connected by the flexible beams which are used to describe the global stiffness of the floater. Hydrostatic ad hydrodynamic loads on each body are calculated by integrating the hydrostatic and hydrodynamic pressure along the corresponding wet surface. The velocity potential is obtained by solving the linear potential-flow boundary value problem with assumption of rigid body for the whole floater. These external loads together with the gravity loads and inertial loads as the integrated loads are implemented in the nodes of finite element model of the flexible floater to carry out a time-domain analysis. No hydroelasticity effects are taken into account in the proposed methodology.

Under constant wind condition, there is no difference in the global dynamic responses between rigid and flexible floater model in all range of wind speed except for the tower base bending moments. In above-rated wind speeds, the amplitude and standard deviation of tower base bending moments in the flexible floater model is over 20% larger than those in the rigid floater model.

Under regular wave condition, the floater motions agree well between the rigid and flexible floater model. For the tower base bending moments and mooring line tensions, there is a good agreement below 0.3 Hz, while for higher frequencies, the responses around the tower

bending natural frequency predicted by the flexible floater model are over 25% smaller compared to the rigid floater model. This difference may be related to the modelling of structural damping in the two models. The floater flexibility also reduces the tower bending natural frequency from 0.41 Hz (rigid floater) to 0.38 Hz (flexible floater).

The floater flexibility has a significant influence on the global dynamic responses around the tower bending natural frequency under irregular wave condition, not only changing the tower bending natural frequency, but also reducing the dynamic responses around tower bending natural frequency. That is consistent with the conclusions under the regular wave condition. The responses in the low-frequency range and the linear wave-excitation show a better agreement. The contributions of the difference-frequency QTFs not only increase the low-frequency dynamic responses, but also results in the increasing of the responses around tower bending natural frequency.

For the irregular wave and turbulent wind condition, at lower mean wind speed, the largest contribution to the dynamic responses comes from the wind frequency component. At higher mean wind speed, the response at the surge or pitch resonance frequency dominates. The floater flexibility has negligible contribution to the responses in the low-frequency and wave frequency range. Similar to the regular and irregular wave condition, the floater flexibility changes the tower bending natural frequency and the responses around the tower bending natural frequency.

In conclusion, the floater flexibility decreases the tower bending natural frequency and has a significant influence on the global dynamic responses around tower bending natural frequency. However, the effect of floater flexibility on the responses in the low-frequency and wave frequency range is negligible.

CRediT authorship contribution statement

Haoran Li: Conceptualization, Methodology, Software, Validation, Investigation, Formal analysis, Data curation, Writing – original draft. **Zhen Gao:** Conceptualization, Methodology, Formal analysis, Resources, Writing – review & editing, Supervision. **Erin E. Bachynski-Polić:** Formal analysis, Writing – review & editing. **Yuna Zhao:** Software, Investigation, Data curation. **Stian Fiskvik:** Software, Investigation, Data curation.

Declaration of competing interest

The authors declare that they have no known competing financial interests or personal relationships that could have appeared to influence the work reported in this paper.

Data availability

Data will be made available on request.

Acknowledgements

The financial support provided by the COWI Foundation through the EMULF project is gratefully acknowledged by the authors.

References

Abbas, N.J., Wright, A., Pao, L., 2020. An update to the National Renewable Energy Laboratory baseline wind turbine controller. In: Journal of Physics: Conference Series. IOP Publishing, 012002.

Allen, C., Viscelli, A., Dagher, H., Goupee, A., Gaertner, E., Abbas, N., Hall, M., Barter, G., 2020. Definition of the UMaine VolturnUS-S Reference Platform Developed for the IEA Wind 15-megawatt Offshore Reference Wind Turbine. National Renewable Energy Lab.(NREL), Golden, CO (United States).

Borg, M., Bredmose, H., Hansen, A.M., 2017. Elastic deformations of floaters for offshore wind turbines: dynamic modelling and sectional load calculations. In: International Conference on Ocean, Offshore and Arctic Engineering. American Society of Mechanical Engineers.

Borg, M., Hansen, A.M., Bredmose, H., 2016. Floating substructure flexibility of large-volume 10MW offshore wind turbine platforms in dynamic calculations. In: Journal of Physics Conference Series. IOP Publishing, 082024.

Cao, Q., Xiao, L., Cheng, Z., Liu, M., 2021. Dynamic responses of a 10 MW semi-submersible wind turbine at an intermediate water depth: a comprehensive numerical and experimental comparison. Ocean Eng. 232, 109138.

Chen, Z., Wang, K., Gao, Z., Moan, T., 2017. A comparative study on dynamic responses of spar-type floating horizontal and vertical axis wind turbines. Wind Energy 20 (2).

Commission, I.E., 2009. IEC 61400-3 Wind Turbines Part3: Design Requirements for Offshore Wind Turbines. International Electrotechnical Commission, Geneva, Switzerland.

DNV, G., 2016. Design of Offshore Steel Structures, General (LRFD Method). DNVGL-OS-C101.

DNV, G., 2017. Offshore Standards (OS).“Structural Design of Offshore Units–WSD Method”. DNVGL-OS-C201.

DNV, G., 2018. Offshore Standards (OS).“Structural Design of Column Stabilised Units–LRFD Method”. DNVGL-OS-C103.

Europe, W., 2017. Floating Offshore Wind Vision Statement. Brussels,Belgium.

Gaertner, E., Rinker, J., Sethuraman, L., Zahle, F., Anderson, B., Barter, G.E., Abbas, N.J., Meng, F., Bortolotti, P., Skrzypinski, W., 2020. IEA Wind TCP Task 37: Definition of the IEA 15-megawatt Offshore Reference Wind Turbine. National Renewable Energy Lab.(NREL), Golden, CO (United States).

Henderson, A.R., Argyriadis, K., Nichols, J., Langston, D., 2010. Offshore Wind Turbines on TLPs–Assessment of Floating Support Structures for Offshore Wind Farms in German Waters. 10th German Wind Energy Conference, Bremen, Germany, pp. 1–5.

Hofmann, M., Sperstad, I.B., 2014. Will 10 MW wind turbines bring down the operation and maintenance cost of offshore wind farms? Energy Proc. 53, 231–238.

Laboratory, N.R.E., 2019. ROSCO, Version 0.1.0.

Lee, C., 1995. Theory Manual.

Li, H., Hu, Z., Wang, J., Meng, X., 2018. Short-term fatigue analysis for tower base of a spar-type wind turbine under stochastic wind-wave loads. Int. J. Nav. Archit. Ocean Eng. 10 (1).

Li, L., Hu, Z., Wang, J., Hu, Q., 2014. Dynamic responses of a semi-type offshore floating wind turbine. In: International Conference on Ocean, Offshore and Arctic Engineering. American Society of Mechanical Engineers.

Lloyd, D.N.V.G., 2010. Recommended Practice DNV-RP-C201—Environmental Conditions and Environmental Loads. DNV GL: Høvik, Norway.

Luan, C., 2018. Design and Analysis for a Steel Braceless Semi-submersible Hull for Supporting a 5-MW Horizontal axis Wind Turbine. Norwegian University of Science and Technology.

Luan, C., Gao, Z., Moan, T., 2016. Design and Analysis of a Braceless Steel 5-MW Semi-submersible Wind Turbine, International Conference on Offshore Mechanics and Arctic Engineering. American Society of Mechanical Engineers.

Luan, C., Gao, Z., Moan, T., 2017a. Development and verification of a time-domain approach for determining forces and moments in structural components of floaters with an application to floating wind turbines. Mar. Struct. 51, 87–109.

Luan, C., habaud, V.C., Bachynski, E.E., Gao, Z., Moan, T., 2017b. Experimental validation of a time-domain approach for determining sectional loads in a floating wind turbine hull subjected to moderate waves - ScienceDirect. Energy Proc. 137, 366–381.

MANUAL, S.U., 2017. Wave Analysis by Diffraction and Morison Theory.

MARINTEK, 2012. SIMO—Theory Manual Version 4.0. MARINTEK, Trondheim, Norway.

Moan, T., Gao, Z., Bachynski, E.E., Nejad, A.R., 2020. Recent advances in integrated response analysis of floating wind turbines in a reliability perspective. J. Offshore Mech. Arctic Eng. 142 (5), 1–73.

Musial, W., Spitsen, P., Duffy, P., Beiter, P., Marquis, M., Hammond, R., Shields, M., 2022. Offshore Wind Market Report, 2022 Edition. National Renewable Energy Lab. (NREL), Golden, CO (United States).

Ormberg, H., Passano, E., 2012. RIFLEX Theory Manual. Marintek.

Sagar, H., Ley, J., Moctar, B., 2015. Hydroelasticity effects of wave induced loads on offshore monopile structure. In: 7th International Conference on Hydroelasticity in Marine Technology, Split, Croatia, pp. 82–101.

Souza, C.E.S.d., Bachynski, E.E., 2018. Effects of hull flexibility on the structural dynamics of a TLP floating wind turbine. In: International Conference on Offshore Mechanics and Arctic Engineering. American Society of Mechanical Engineers.

Suja-Thauvin, L., Krokstad, J.R., Bachynski, E.E., 2018. Critical assessment of non-linear hydrodynamic load models for a fully flexible monopile offshore wind turbine. Ocean Eng. 164, 87–104.

Suja-Thauvin, L., Krokstad, J.R., Bachynski, E.E., Ridder, E., 2017. Experimental results of a multimode monopile offshore wind turbine support structure subjected to steep and breaking irregular waves. Ocean Eng. 146, 339–351.

Takata, T., Takaoka, M., Gonçalves, R.T., Houtani, H., Yoshimura, Y., Hara, K., Oh, S., Dotta, R., Malta, E.B., Iijima, K., 2021. Dynamic behavior of a flexible multi-column FOWT in regular waves. J. Mar. Sci. Eng. 9 (2), 124.

Veritas, D.N., 2010. Buckling Strength of Shells, Recommended Practice DNV-RP-C202. Det, vol. 1. Nor. Ver. Class. AS, Veritasveien.

Wang, H., Hu, Z., Meng, X., 2018. Dynamic performance investigation of a spar-type floating wind turbine under different sea conditions. China Ocean Eng. 32 (3).

Zhao, Y., Yang, J., He, Y., 2012. Preliminary design of a multi-column TLP foundation for a 5-MW offshore wind turbine. Energies 5 (10).